Journal of Disability Research

2023 | Volume 2 | Issue 1 | Pages: 85–97
DOI: 10.57197/JDR-2023-0011

Exploring Orthosis Designs for 3D Printing Applying the Finite Element Approach: Study of Different Materials and Loading Conditions

Usama Umer[1,2,*], Syed Hammad Mian[1,2], Khaja Moiduddin[1,2] and Hisham Alkhalefah[1,2]

[1]Advanced Manufacturing Institute, King Saud University, Riyadh 11421, Saudi Arabia
[2]King Salman Center for Disability Research, Riyadh 11614, Saudi Arabia

Correspondence to:
U. Umer*, e-mail: uumer@ksu.edu.sa, Tel.: +966-11-8063573

Received: March 29 2023; Revised: May 28 2023; Accepted: May 28 2023; Published Online: June 15 2023

ABSTRACT

Three-dimensional (3D) printing, especially using fused deposition modeling, is becoming more and more popular in the medical sector because of its exceptional advantages. While it has been used for prototyping, 3D printing has not yet been completely explored to produce a functional product. The key causes are the abundance of 3D printing materials and the lack of a comprehensive study outlining the design process. Consequently, this paper describes a reverse engineering (RE) design approach based on data acquisition utilizing laser scanning and splint design from the acquired point cloud data. This study also focuses on the evaluation of various wrist orthosis/splint designs and materials using finite element (FE) analysis in order to improve upon the conventional approach. Sixty FE analysis simulations are undertaken in flexion–extension and radial–ulnar wrist movements to investigate the displacements and the stresses. The splint is then fabricated utilizing the material and thickness that have been specified by FE analysis. The major goals of this study are to examine the RE design methodology, explore various materials, and assess the viability of 3D printing. The polylactic acid (PLA) hand splint has proven to be the sturdiest in terms of average displacements when compared to the other materials, followed by polyethylene terephthalate glycol (PETG), acrylonitrile butadiene styrene (ABS), polypropylene, and thermoplastic polyurethanes. According to simulation data, the PLA splint has 38.6%, 38.8%, 38.5%, and 38.7% less displacement in the major loading direction in flexion, extension, radial, and ulnar, respectively, than the ABS splint. Moreover, the PLA-based hand splint has a peak stress value below the yield strength of PLA, rendering it reliable for patients to wear. Also, it turns out that PETG and ABS behave rather similarly. Furthermore, it has been shown that a balanced approach can reduce material use and building time. For instance, employing PLA and a thickness of 2 mm results in reduced material costs without compromising the effectiveness of the splint. As a result, choosing the right material and splint thickness can help the 3D-printed hand splint perform better.

KEYWORDS

stroke, hand splint/orthosis, finite element analysis, reverse engineering, 3D printing

INTRODUCTION

Stroke is a serious cerebrovascular illness that affects adults all over the world and causes high mortality and long-term impairment. Stroke is the second most common cause of mortality and the third leading cause of disability globally and a significant contributor to morbidity (Robert and Zamzami, 2014). Research demonstrates that there are numerous reasons and influencing variables that result in a high cost for people with disabilities (Abdelbasset and Sulieman, 2022). Stroke survivors are frequently left with severe mental and physical disabilities that place a significant social and economic burden on the society. The Kingdom of Saudi Arabia, which is the largest nation in the Middle East region, is home to more than 28 million people and occupies roughly four-fifths of the Arabian Peninsula. The combined annual incidence of stroke in Saudi Arabia is 29–43.8 strokes per 100,000 individuals per year (Alqahtani et al., 2020; Bakraa et al., 2021). More than half of stroke survivors have chronic upper limb deficits, such as loss of strength and dexterity, stiffness, muscular contracture, discomfort, and edema (Broeks et al., 1999). In patients with stroke and a nonfunctional spastic upper limb, many methods are employed to inhibit spasticity, avoid contractures, alleviate discomfort and edema, or improve hygiene. However, there is no consensus on the most effective treatment, but on the best course

of action, long-term splinting using static orthoses is the most frequent and accepted intervention so far (Miller et al., 2010; Andringa et al., 2013).

Static progressive orthoses is a special type of immobilization splint used by the therapist to assist the patient in regaining the passive range of motion (PROM) joints (Schultz-Johnson, 2002). It uses a nonelastic component that exerts a force on a stiff joint to tighten the tissue for remodeling. Upon fabrication, the static progressive orthosis allows the wearer to provide minor incremental changes in the joint position as the PROM of the stiff joint gives away gradually. Typically, these splints are commonly worn 3–4 times daily for 30 minutes to reap the benefits of the low-load force application (Bhave et al., 2019). There are several studies supporting the benefits of static progressive orthosis, which include the following (Schultz-Johnson, 2002):

(a) Increase in the range of motion without discomfort. A stiff joint is under tension from a nonelastic component to retain its highest tolerable length.
(b) It is possible to adjust the tension force gradually for each finger by the wearer. The longer the tissues stay at their maximum acceptable length, the longer they grow.
(c) Gradual improvements of 5–10° per week can be used to gauge the success of orthosis.

Static progressive orthosis can be acquired as a prefabricated device as "off the shelf" or can be custom-made as per the patient's anatomical structure. The traditionally obtained commercial prefabricated orthoses rely on a "one-size-fits-all" approach and therefore cannot be customized to fit a particular person unless they are modified by the user or an orthotic specialist. In addition, poorly fitted orthoses lead to directional misalignment and shear stress over bone prominences. Another significant drawback observed is the material thickness and restricted perforation, which could cause excessive sweat, encourage the growth of germs, and result in an offensive, unclean, and odorous orthosis. Patients accepting such prefabricated orthoses frequently fail due to their impractical hygiene and aesthetics issues. Studies reveal that two-thirds of the patients wearing prefabricated orthoses report noncompliance with their devices. Aesthetics play a significant role in influencing the adoption or abandonment of the device (Luximon et al., 2019; Barrios-Muriel et al., 2020).

The use of three-dimensional (3D) printing techniques in orthopedic and rehabilitation practice has generated a lot of discussions recently as they make it feasible to design orthoses and enhance patient treatment satisfaction levels. 3D printing through the digital manufacturing process has mainly benefited the produced orthosis devices. With 3D scanning, highly personalized patient-specific orthoses can be produced with accurate fit and comfort. 3D printing enables the direct fabrication of parts from 3D model data, in a layer-by-layer fashion thus eliminating the auxiliary resources used in traditional fabrication. When compared to traditional manufacturing methods, 3D printing significantly reduces material waste, shortens manufacturing times, and solves many issues caused by traditional manufacturing processes (Aimar et al., 2019).

Over the past few years, 3D printing is expanding rapidly and there have been numerous applications of 3D printing in a variety of fields including the biomedical industry (Mian et al., 2022). The global market for 3D printing in healthcare is anticipated to reach $2.5 billion by the end of 2023, expanding at a compound annual growth rate of 21.2% (MedScan3D, 2023). 3D printing thus satisfies the long-felt need of functional, aesthetic, and user-fit requirements for orthotic devices, thus becoming a viable option. There are a variety of materials used for printing orthotic devices, like acrylonitrile butadiene styrene (ABS), polypropylene (PP), polycarbonate, acrylic, carbon fiber, and polylactic acid (PLA). Walbran et al. (2016) in their study compared the yield stress of custom-made orthotic devices fabricated through 3D printing using nylon, carbon, and PLA. Similarly, Paton et al. (2007) investigated the physical characteristics of soft materials such as ethylene vinyl acetate and poron to create orthoses to prevent neuropathic diabetic foot ulcers. Blaya et al. (2018) in their study proposed a 3D digitalization methodology where reverse engineering (RE) was utilized to design and print a splint model using polycarbonate and PLA material. Strength, elasticity, hardness, density, temperature response, durability, flexibility, compressibility, and resilience are only a few of the physical characteristics of the orthosis material (Vaish and Vaish, 2018). It should be noted that one physical characteristic cannot be used to evaluate a material for an orthotic device on its own. An inappropriate material and a poor design could lead to an uncomfortable device or an orthotic device that is biomechanically harmful.

A biomechanical study using finite element (FE) analysis helps to examine the mechanical behavior of the designed orthoses under different loading and other boundary conditions for various materials. The FE technique offers tremendous time and cost savings for assistive devices such as orthoses (or splints), prosthetics, etc., that need to be modified and checked regularly for different materials and thicknesses (Kubasad et al., 2020; Siddiqui et al., 2023). FE analysis predicts the success and failure of the 3D model by studying the biomechanical properties, thus simulating real-world scenarios. Together with contemporary technologies such as 3D scanning and 3D printing, the FE approach is still extensively employed in the creation of novel orthosis designs (Choi et al., 2019; Lu et al., 2021). Li and Tanaka (2018) performed the FE analysis on the different splint models to evaluate the structural strength and assess the wearing experience. Cazon et al. (2017) utilized FE analysis to evaluate additive manufacturing (AM) wrist splints and enhance the traditional splinting strategy. Łukaszewski et al. (2020) compared the experimental and simulation study on the ABS material properties of the customized wrist orthoses produced using the fused deposition modeling (FDM) method.

This study thus focuses on the integration of 3D scanning, FE analysis, and 3D printing to obtain a patient-specific splint for upper limb paresis. A set of five different materials is simulated under flexion–extension and radial–ulnar wrist movements to investigate the displacements and the stresses. The goal of this study is to use FE analysis to select an appropriate material and orthosis design that can meet the long-felt need for functional and aesthetic requirements.

MATERIALS AND METHODS

This study establishes a framework (Fig. 1) that encompasses data acquisition, an RE design strategy (or modeling technique), a numerical analysis procedure, and fabrication technology. This study compares different wrist splint designs based on various thicknesses and materials using FE.

Data acquisition

The hand splint modeling process uses the 3D data from the laser scanning device as its input. Data collection is done using a healthy volunteer's hand from the research team. One of the most crucial procedures in this method is the collection of anthropometric data on the subject's limb. The scanning is carried out using the Faro Platinum arm (FARO, Lake Mary, FL, USA), as depicted in Figure 2a. The purpose of 3D scanning is to obtain the subject's Standard Tessellation Language (STL) file, which is deployed to design the custom splint using RE (as seen in Fig. 2b).

Laser scanning is used to digitize the subject (or limb) in 3D space, to obtain as much surface area as possible to increase design freedom. The upper limb (or hand) is stretched as nearly as it can go without feeling tight or painful in order to put the subject in a comfortable position. The limb is relaxed during the scanning process to allow for passive muscle stretching. During data collection, if the limb is stretched out too far, the subject may feel discomfort.

The ideal scanning results can be obtained by meticulously adjusting the scanner parameters (Mian and Al-Ahmari, 2019). For instance, slow scanning speeds may cause errors from unintentional movements, but faster scanning rates may cause the scanner to overlook some portions. It is also imperative to modify the acquisition settings of the sensor to account for surface texture, surface color, and lighting effects. Maintaining a safe distance from the surface being scanned is also necessary for optimal scanning. Efficacious scanning requires a number of key factors, such as the scan rate, scan density, exposure time, noise threshold, data format, etc., to be appropriately defined. The interpretation of scan rate is the number of scan lines per second, and a value of 30 is chosen in this study (see Table 1). The value of scan density which means how many points are featured on each scan line is selected as 640 points. The device uses the surface form and reflectivity of the object being scanned to autonomously establish the laser's exposure settings. The noise threshold is a nondimensional item that measures the level of noise in the data. Based on the surface and the environment, the software selects the noise threshold value automatically. Each pixel that the laser line scanner sends onto the surface is assessed for intensity or return power. The term "noise" or "chatter" refers to all data whose intensity is below the noise threshold value. A point cloud with a persistent density and points arranged in straight rows and columns represents the organized data. A point cloud with a variable density made up of points at each spot the laser line scanning probe discovers on the object is the unordered (or raw) data. Prior to starting the scanning procedure, the various parameters shown in Table 1 are specified.

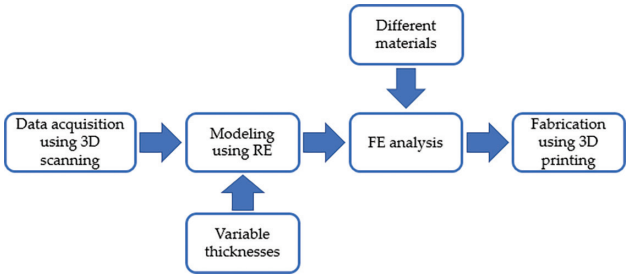

Figure 1: Approach adopted to realize the hand splint. Abbreviations: 3D, three-dimensional; FE, finite element; RE, Reverse Engineering.

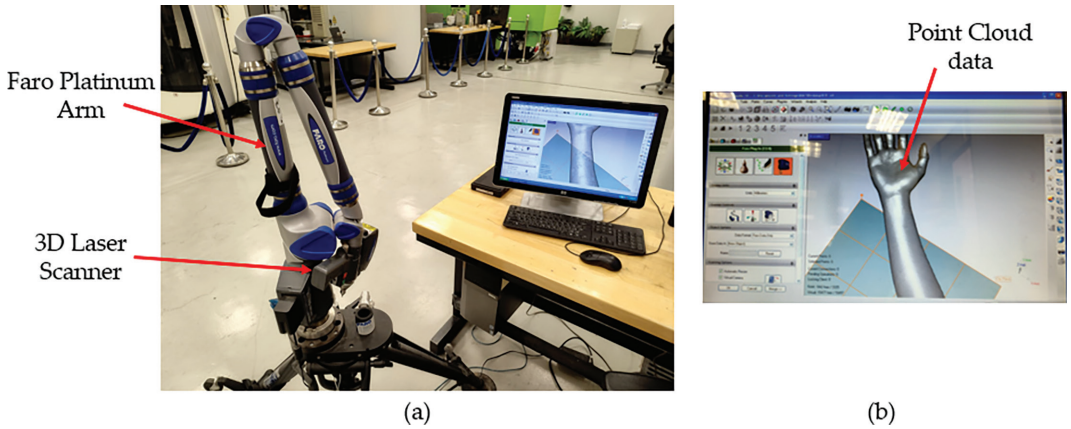

Figure 2: (a) 3D scanning system; (b) acquired point cloud data. Abbreviation: 3D, three-dimensional.

Table 1: Scanning parameters for data acquisition.

Scan rate	30 scan lines/second	Scan density	640 points/scan line	Noise threshold	15
Time of exposure	21 millisecond	Data format	Raw data		

The polygon model contains error elements such as erroneously recorded surfaces, missing faces from the desired regions, etc. The file is therefore cleaned, optimized, and made ready for the subsequent design and modeling phase in order to improve the efficiency of the splint design procedure. The following procedures are also carried out: noise and outlier removal, faulty facets cleanup, mesh refining and smoothing, hole filling, and face error elimination. The generated polygon model in Figure 3c is then saved in the STL format to model and create 3D splints.

Design and modeling

The following action is to develop a custom hand splint model using the mesh template (STL file) (Fig. 4a). The cornerstone for building a splint model that is customized to the subject's hand form is the adoption of interpolation spline curves (Wyleżoł, 2018). With CATIA V5, various modules, including the Digitized Shape Editor, Generative Shape Design, and Quick Surface Reconstruction, are combined to complete the modeling process. The approach proposed is universal and can be used regardless of the limb, whether

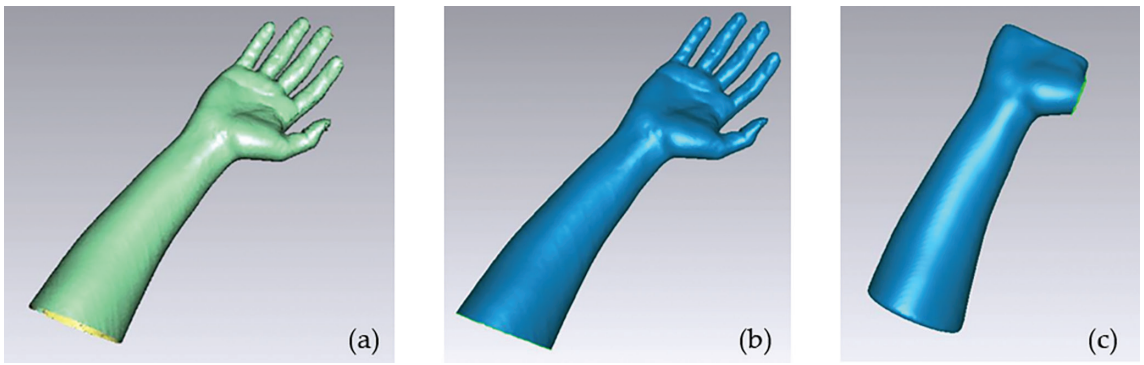

Figure 3: Scanning outcome: (a) point cloud, (b) generated mesh, and (c) mesh prepared for splint design.

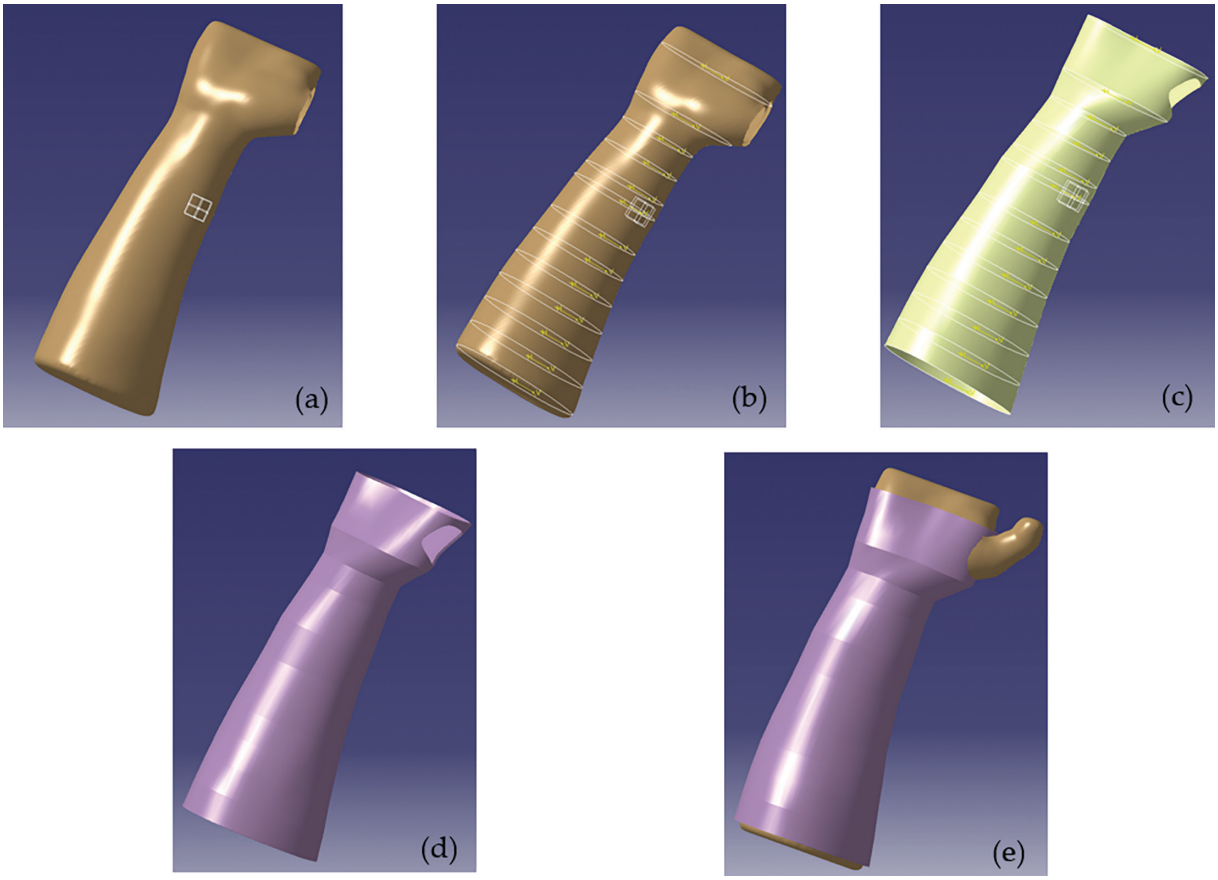

Figure 4: Modeling of the hand splint: (a) mesh of the hand (STL file), (b) recognition of curves on the mesh, (c) surface acquired through curves, (d) conversion of surface to part model, and (e) splint placed on the mesh. Abbreviation: STL, Standard Tessellation Language.

it is an upper or a lower limb. The first stage of the modeling process is defining the spline curves encompassing the surface of the hand in the Digitized Shape Editor as shown in Figure 4b. For this reason, the Planar Sections option is preferred. It approximates curves by employing planes to cut a mesh or a cloud of points. The shape of the curves is interpolated among the existent neighboring nodes whenever the curves are detached, resulting in a spline curve that smoothly traverses all of the necessary points. To do this, a bridging curve spanning two curves is constituted using the Connect Curve option in Generative Shape Design. The resulting spline curves are then used to enable surface patching. The Quick Surface Reconstruction environment of the CATIA V5 system is exploited to carry out the surface-generating procedure. The surface patch is constructed following the spline curve's curvature using the multisection surface method (Fig. 4c). The hole at the location of the thumb is then created using the split command in the Generative Shape Design. The procedure culminates with the transition of the splint surface model into the part model, as shown in Figure 4d. The splint is carefully positioned on the hand mesh or template, as can be seen in Figure 4e.

FE analysis

This study focuses on using FE analysis to compare various wrist splint designs and materials. The methodology put forth by Cazon et al. (2017) served as the foundation for FE analysis used in this paper. In the present work, the design consists of splints with different thicknesses (1, 2, and 3 mm), and different materials comprising PLA, ABS, thermoplastic polyurethanes (TPU), PP, and polyethylene terephthalate glycol (PETG) are considered. With the superior rigidity of the AM material in mind, these thicknesses are deemed reasonable. The properties of these materials to be used in the FE model shown in Table 2 have been obtained from the literature and online resources.

The software used for FE analysis is Abaqus from Dassault Systems (Dassault Systems Headquarters, Vélizy-Villacoublay, France). The designed splint is imported into Abaqus via the Initial Graphics Exchange Specification file format. The FE model is generated and resulted in 11,481 node points and 37,225 linear four-node tetrahedral elements (C3D4) for the splint (Fig. 5).

There are four wrist movements as a result of the wrist's primarily biaxial mobility at the region of the carpus: flexion–extension and radial–ulnar deviation (Youm et al., 1978; Volz et al., 1980). Typically, individuals who have undergone static (isometric) and dynamic (isokinetic) tests are employed to determine the wrist strength involved in each of these motions. In this work, the greatest flexion–extension torque and radial–ulnar deviation torque reported by Vanswearingen (1983) that healthy volunteers could produce are taken into consideration. In actual conditions, it seems doubtful that individuals with strokes would frequently be able to exert the full force that could ultimately shatter the splint. Because of this, the analyses in this study are carried out at 8% of a competent person's maximal isometric strength. However, the FE simulations are also run with 12% of the peak isometric strength of a healthy person to imitate the more aggravated condition. Table 3 lists the loads and torques that have been applied on the splint for the four major movements.

The input force (N) required for the simulation is derived by dividing the torque by the length between the wrist and the metacarpophalangeal joints (Glinsky et al., 2008). It is presumed that the distance between the wrist and the metacarpophalangeal joints is 0.1 m, given that 50% of the participants (without any hand-wrist disorders) had this measurement (Garrett, 1971). The estimated force values (Table3) are assigned to the splint surfaces that are potential contenders to carry such forces in real life. It is significant to prevent stress concentrations caused by point forces and to portray a more natural interplay involving the splints and the hand/wrist. Figure 5a-d presents the FE mesh, boundary conditions, and load directions for the four main wrist movements, including flexion, extension, radial, and ulnar, respectively. It is extremely important to recognize that the regions in contact with the thumb are also taken into account for the radial movement while the palm portion is only taken into account for the ulnar movement, in addition to the most evident surfaces under loads depending on each movement. The patient's forearm is theorized to be at repose (or fixed) for the simulations, while the hand is free to move but is constrained by the splint. In this manner, the boundary condition is to firmly link the surfaces of the splint at the forearm area (three translations and three rotations). The back surfaces of the splint are fixed in 6 degrees of freedom (DOF) for each of the four movements. In order to align the simulated

Table 2: Properties of the 3D printing materials.

Material	Properties		
	Young's modulus (MPa)	Poisson ratio	Yield strength (MPa)
PLA	3466 (Oksiuta et al., 2020)	0.30 (Oksiuta et al., 2020)	60 (Travieso-Rodriguez et al., 2019; Sepahi et al., 2021)
ABS	2100 (Yavuz et al., 2021)	0.35 (Yavuz et al., 2021)	45 (Vukasovic et al., 2019; OMNEXUS)
TPU	28.5 (León-Calero et al., 2021; Krumm et al., 2022)	0.39	34 (León-Calero et al., 2021)
PP	1070 (Chen et al., 2022)	0.42 (Chen et al., 2022)	30 (Handayani et al., 2021)
PETG	2200 (Huysamen et al., 2020; PETG, nd)	0.33 (Huysamen et al., 2020)	50 (PETG, nd; PETG 3D, nd; Keane, 2021)

Abbreviations: ABS, acrylonitrile butadiene styrene; PETG, polyethylene terephthalate glycol; PLA, polylactic acid; PP, polypropylene; TPU, thermoplastic polyurethanes.

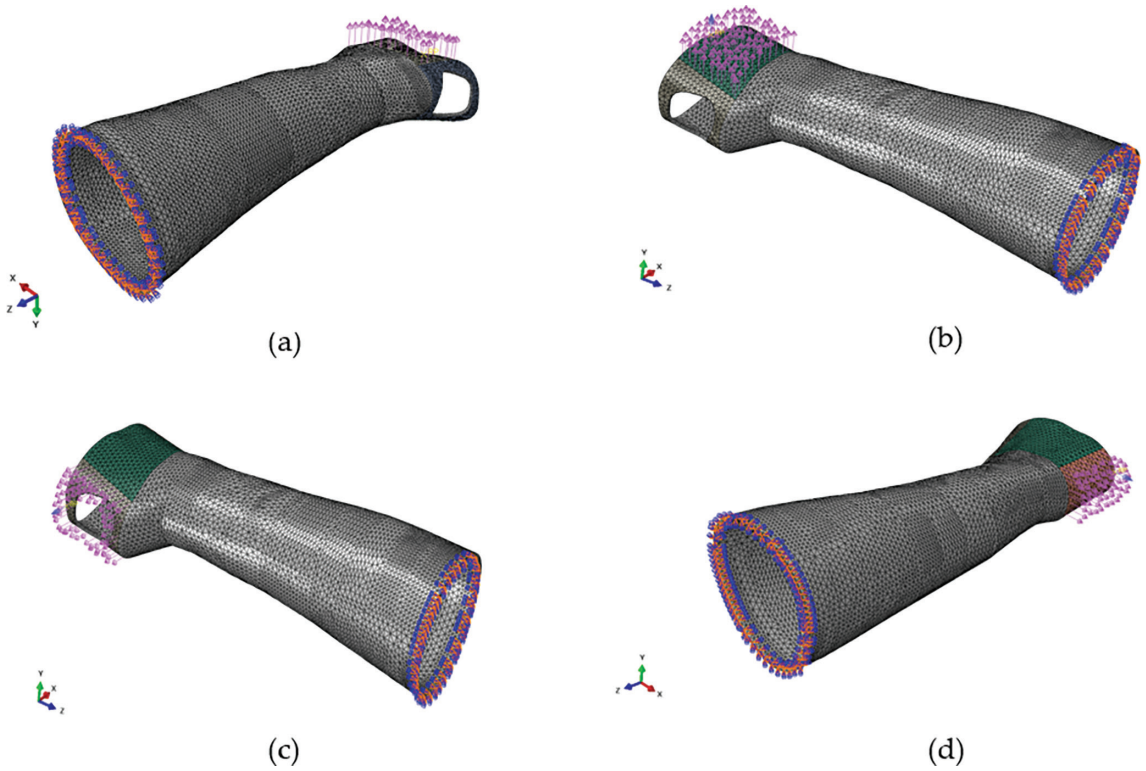

Figure 5: FE mesh, BCs and load directions for the four main wrist movements. (a) flexion, (b) extension, (c) radial, and (d) ulnar. Abbreviations: BC, boundary condition; FE, finite element.

Table 3: Considered torque and loads applied to the splints.

	Vanwearingen torque (N m)	Applied 8% loads (N)	Applied 12% loads (N)	Load direction
Flexion	14.8	11.8	17.8	–Y-axis
Extension	8.4	6.7	10.1	Y-axis
Radial deviators	11.4	9.1	13.7	–X-axis
Ulnar deviators	9.9	7.9	11.9	X-axis

forearm–splint interactions with the actual ones and create the three-point pressure system, each motion also has a secondary limit placed on the center surfaces of the splint.

Sixty FE analysis simulations are undertaken in flexion–extension and radial–ulnar wrist movements to investigate the displacements and the stresses. These simulations examine the influence of the different thicknesses on the splint as well as the performance of the different materials. All simulations consider small deformations, which means the materials stay in their elastic region of the stress–strain curve. The simulations are performed via a static, all-encompassing process that makes use of the implicit solver in ABAQUS/STANDARD. These analyses estimate and contrast the displacements and the von Mises stress. All simulations are executed on a PC with an Octa-core Xeon processor running at 3.7 GHz, 16 GB of RAM, and Windows 10, 64 bits. Each simulation needs approximately 1 minute.

Fabrication of the splint

The manufacture of the modeled splint begins by correcting issues with the STL file. Magics® 18.0 (Materialise NV, Leuven, Belgium, 2013) is used to fix problems including overlapped, intersecting triangles, twisted corners, and other errors. The objective of this stage is to set up the STL file by specifying the ideal position and orientation for manufacturing as well as generate the supports wherever needed for optimal manufacturing. Appropriate supports are required in order to build the prototype accurately and without any abnormalities. Moreover, they are needed for effective heat transfer and to avoid deformation. INTAMSUITE slicing software (version 3.6.2; INTAMSYS Technology Co. Ltd, Shanghai, China) is utilized to slice, orient, and generate supports for the fabrication of the 3D model using a Funmat HT 3D printer, as shown in Figure 6.

The customized hand splint is produced using an INTAMSYS (Intelligent Additive Manufacturing Systems) FUNMAT HT 3D printer (INTAMSYS Technology Co. Ltd) (INTAMSYS, nd). The built-in slicing software INTAMSUITE (INTAMSYS Technology Co. Ltd) is used to convert the STL splint file into a G-code which is then transferred into the Funmat HT 3D printer using an SD card. The printer employs FDM technology, which, when the printing settings are adjusted properly, has the benefit of applying lower energy, yielding more, and delivering superior tensile strength (Petousis et al., 2023). FDM is one of the most used

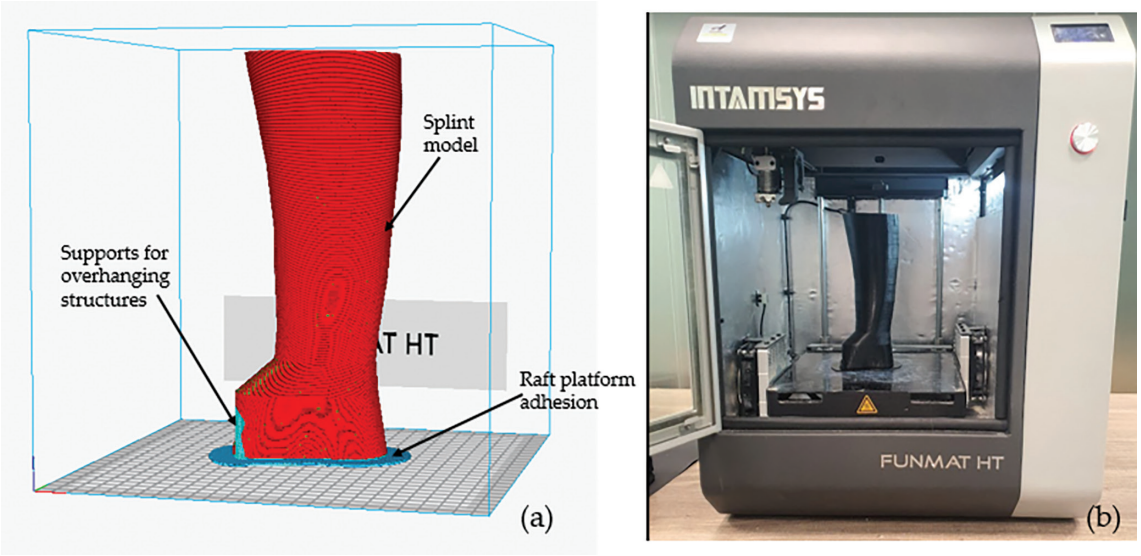

Figure 6: (a) INTAMSUITE software for the orientation and support generation of the 3D model and (b) fabrication of hand splint using Funmat HT Printer. Abbreviation: 3D, three-dimensional.

and simple AM techniques (Lalegani Dezaki et al., 2021). The printer has two nozzle extruders, one the standard temperature nozzle for engineering materials such as PLA, ABS, Polyamide (PA), Polycarbonate (PC), High Impact PolyStyrene (HIPS), TPU, etc., and the other high-end nozzle for high-temperature polymers such as Polyether ether ketone (PEEK), Polyetherketoneketone (PEKK), Ultem® (polyetherimide) (ULTEM), etc. (INTAMSYS, nd). The extruder nozzle is an adjuster as per the selection of material used for printing. Many variables affect how 3D-printed objects are produced. So, it is crucial to choose the right specifications while fabricating any component. Table 4 provides the process variables applied to splint production. The printer has a heated build plate of high borosilicate glass that can withstand temperatures of up to 160°C and a build chamber that can reach temperatures of up to 90°C. The infill density of slicing software is set to 100% to create a perfectly solid and durable construction.

Table 4: Process variables used in the FUNMAT HT 3D printer.

Description	3D printer settings (INTAMSYS, nd)
Printing technology	FDM
Build platform	High borosilicate glass
Connectivity	SD card
Extruder nozzle diameter	0.4 mm
Layer thickness	0.1 mm
Print speed	60 mm/s
Extruder temperature	220°C
Chamber temperature	50°C
Platform temperature	50°C
Filament diameter	1.75 mm
Input file	STL
Infill density	100%

Abbreviations: 3D, three-dimensional; FDM, fused deposition modeling; STL, standard tessellation language.

The stripping and peeling away of the support structures is a part of the post-processing of any 3D-printed splint. To facilitate easy breaking, the wall of the support structure has been made less thick. Protective gloves are worn while using cutting and gripping pliers to reach the support's undersides and gently bend them upward to eliminate them. It takes about 50.85 m of material and approximately 34 h and 11 minutes to print the splint. The time taken to remove supports has been in-between 5 and 10 minutes. Figure 7a shows a customized splint that has been 3D printed with supports, and Figure 7b shows the final splint after the removal of the supports.

RESULTS AND DISCUSSION

In this study, a comparison of the various materials for hand splints is undertaken. Tables 5 and 6 present the displacements and von Mises stress values, respectively, for the 2-mm-thick hand splint derived from the FE simulations for the 8% load. The absolute displacements and von Mises stress values are also graphically depicted in Figures 8 and 9, respectively.

When compared to other materials, the PLA hand splint is the most rigid in terms of average displacements, followed by PETG, ABS, PP, and TPU. As can be seen in Table 5, the performance of ABS and PETG is rather comparable. ABS has been used as a baseline to compare other materials because it is the most widely used material in 3D printing due to its wide availability and low cost. The hand splint built of PLA material is found to be more robust and stable than the ABS material with roughly 38.6%, 38.8%, 38.5%, and 38.7% less displacement in flexion, extension, radial, and ulnar directions, respectively. Similarly to this, it has been noted that PETG has performed well in terms of displacement. For instance, it has been found that in flexion, extension, radial, and ulnar directions, the PETG-based hand

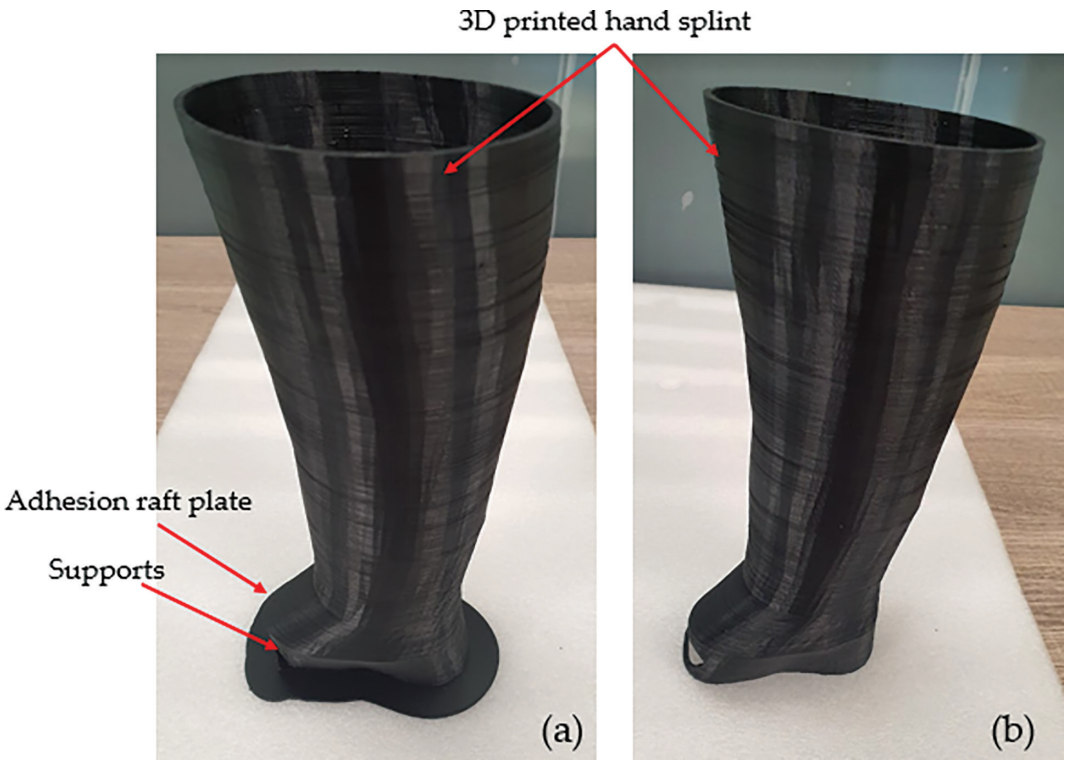

Figure 7: Customized 3D printed splint (a) with supports and (b) post elimination of supports. Abbreviation: 3D, three-dimensional.

Table 5: Highest displacement (mm) attained in the major axes for 8% load.

Material	Flexion (–Y) (mm)	Extension (Y) (mm)	Radial deviators (–X) (mm)	Ulnar deviators (X) (mm)
PLA				
X	0.61	0.18	–0.83	0.81
Y	–2.70	1.28	–0.16	0.18
Z	–0.49	0.28	0.34	–0.28
ABS				
X	0.98	0.29	–1.36	1.33
Y	–4.44	2.11	–0.26	0.29
Z	–0.80	0.46	0.55	–0.46
TPU				
X	69.68	21.12	–100.05	97.49
Y	–324.14	155.11	–18.61	21.45
Z	–57.85	33.60	40.09	–33.33
PP				
X	1.78	0.55	–2.65	2.58
Y	–8.54	4.10	–0.48	0.57
Z	–1.50	0.89	1.05	–0.88
PETG				
X	0.94	0.28	–1.30	1.27
Y	–4.24	2.02	–0.25	0.28
Z	–0.77	0.44	0.53	–0.44

Abbreviations: ABS, acrylonitrile butadiene styrene; PETG, polyethylene terephthalate glycol; PLA, polylactic acid; PP, polypropylene; TPU, thermoplastic polyurethanes.

Table 6: Von Mises stress values (MPa) achieved for 8% load.

Material	Flexion (–Y) (MPa)	Extension (Y) (MPa)	Radial deviators (–X) (MPa)	Ulnar deviators (X) (MPa)
PLA	35.1	15.3	7.50	6.07
ABS	33.38	14.59	7.17	5.93
TPU	31.58	13.87	6.85	5.78
PP	29.64	13.10	6.48	5.61
PETG	34.10	14.88	7.29	5.99

Abbreviations: ABS, acrylonitrile butadiene styrene; PETG, polyethylene terephthalate glycol; PLA, polylactic acid; PP, polypropylene; TPU, thermoplastic polyurethanes.

splint has 4.1%, 4%, 3.9%, and 4.1% fewer displacements than the ABS material. The performance of a hand splint made of TPU, however, has been the worst. Indeed, the ABS material has demonstrated approximately 98.6% lesser displacement than TPU in all flexion, extension, radial, and ulnar directions. The areas of the splints that entail curvature variation, such as the metacarpus, experienced the most displacement regardless of the loading direction. A closer examination of the displacement in each axis revealed that this trend is consistent with the average displacement in flexion, extension, radial, and ulnar movements for all materials.

The PLA splint exhibits stress peaks (35.1 MPa in flexion) in and around the palmer digital region of the hand. The 2-mm-thick PLA-based hand splint is safe to wear by patients with stroke because the peak stress is lower than the yield strength of PLA (60 MPa). The results for the other materials, such as ABS and PETG, are identical, with the exception of PP and TPU, where the peak values are fairly close to their yield strength values. The areas of the splint with curvature and shape variation, such as the sides of the splint, the area around the thumb, etc., both on the palmer and dorsal sides, produce higher stress values. Based on the results of this investigation, particularly the displacement for

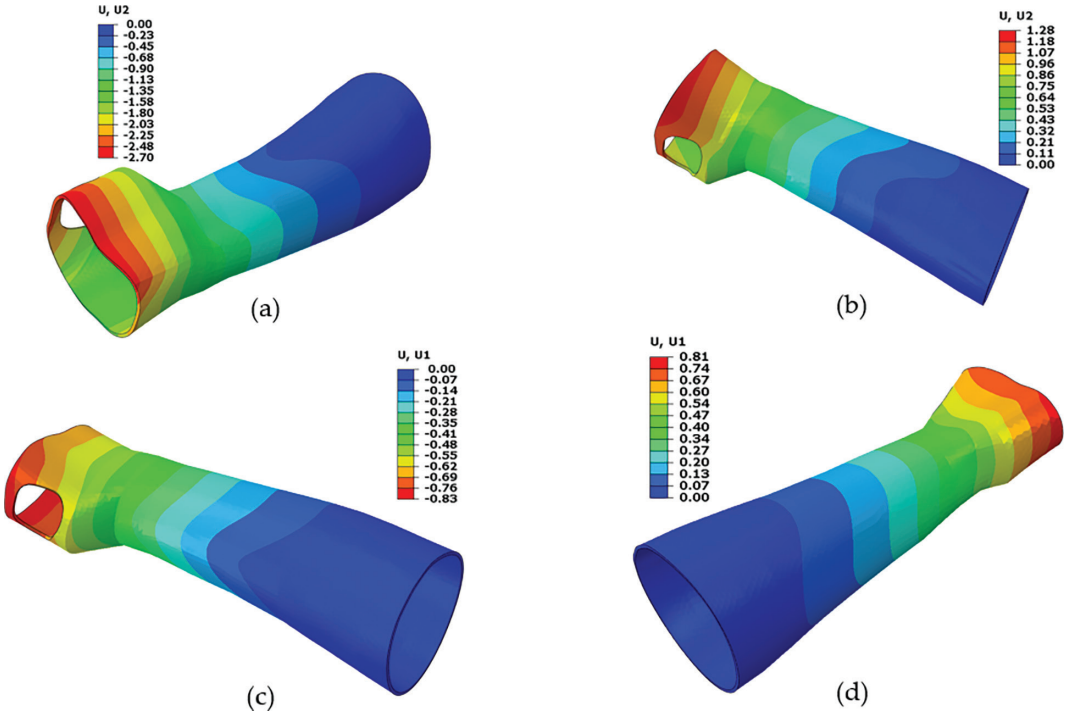

Figure 8: Displacement values (mm) for (a) flexion, (b) extension, (c) radial, and (d) ulnar movements in the 2-mm-thick PLA splint. Abbreviation: PLA, polylactic acid.

a 2-mm-thick splint, it can be said that PLA is the best material for a static hand splint while PP and TPU perform the least. Similarly, it has been noted that the PETG-based hand splint has performed admirably.

The PLA splint has also been subjected to a higher load (i.e., 12% load) to give additional assurance and establish the upper bound of a 2-mm-thick PLA hand splint. The simulation results, which are displayed in Table 7, show that the stated safe behavior of PLA is still present even after increasing the load to 12%.

It is thus demonstrated in Table 7 that when the applied load is 12%, the displacement has undoubtedly resulted in higher deformation. The average displacement has grown rather significantly by 50.1%, 50%, 48.8%, and 47.9% in the flexion, extension, radial, and ulnar directions, respectively. Although the peak stress value has increased by around 50% (as seen in flexion loading), it is still below the yield strength of PLA. The hand splint, however, could break if the load is increased further. Hence, the PLA-based hand splint with a 2-mm thickness would function satisfactorily up until the maximum applied force is 12% of the Vanwearingen torque.

The thickness is both decreased and increased by 1 mm in order to more thoroughly evaluate the PLA-based hand splint. The decrease in the thickness has, of course, naturally led to a reduction in the weight and production costs of the splint. Yet it is discovered that the average displacement under flexion, extension, radial, and ulnar loading has increased dramatically, by roughly more than twofold (see Fig. 10a). Also, it is established as indicated in Figure 10b that when the thickness is reduced by 1 mm, the von Mises stress value (peak stress value of 71.6 MPa in flexion) exceeds the yield strength (60 MPa), implying it has failed to perform.

As a 12% load has been successfully applied to a 2-mm-thick PLA-based hand splint, it is evident that increasing the thickness by 1–3 mm will further enhance its performance. As a result, the load is raised to 20% in order to more accurately assess the PLA-based 3-mm-thick hand splint and identify its load limit. It follows presumably from the increase in thickness that the weight and manufacturing costs of the splint have also increased. For instance, the hand splint with 3-mm thickness would use 27% more material and require a 4.7% longer build time in a 3D printing process. Nonetheless, it has been noted in Table 8 that a 3-mm-thick PLA-based hand splint has performed admirably under higher loads (20% of maximum torque), whereas a 2-mm-thick PLA hand splint will break. Also, the yield strength of the PLA material is higher than the peak stress value of 54.43 MPa. Thus, the thickness of the PLA-based hand splint must be increased to 3 mm if the applied load exceeds 17.8, 10.1, 13.7, and 11.9 N in the flexion, extension, radial, and ulnar movements, respectively. The PLA-based 3-mm hand splint does, however, have a limit on the applied load; specifically, it is anticipated to fail if the applied load exceeds 29.6, 16.8, 22.8, and 19.8 N in the flexion, extension, radial, and ulnar movements, respectively. Consequently, it contributes to the fact that the design and material are the essential aspects to address while designing a dependable hand splint.

Furthermore, the TPU-based hand splint's design is improved by making it 3-mm thick, which may enhance its performance. The comparison of the results (2-mm and 3-mm thickness) for displacement and von Mises stresses is shown in Figure 11a and b. The average displacement has decreased by almost 45%, 43%, 42%, and 38%, respectively, in the cases of flexion, extension, radial, and ulnar loading.

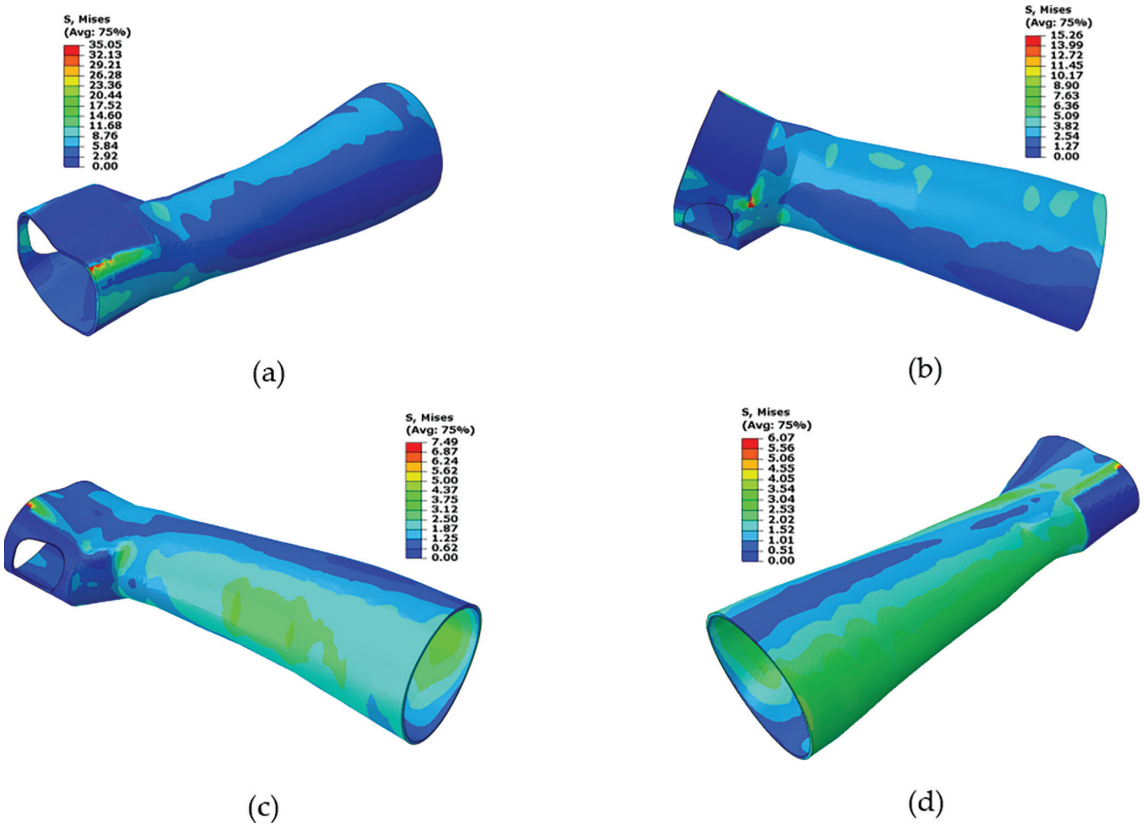

Figure 9: von Mises stress values (MPa) for (a) flexion, (b) extension, (c) radial, and (d) ulnar movements in the 2-mm-thick PLA splint. Abbreviation: PLA, polylactic acid.

Table 7: Summary of the outcomes for 8% and 12% of the imposed load in the 2-mm-thick PLA splint.

PLA	X (mm)	Y (mm)	Z (mm)	von Mises stress (MPa)
Applied load				
8%				
Flexion	0.61	–2.7	–0.49	35.1
Extension	0.18	1.28	0.28	15.3
Radial	–0.83	–0.16	0.34	7.5
Ulnar	0.81	0.18	–0.28	6.07
12%				
Flexion	0.91	–4.05	–0.74	52.58
Extension	0.27	1.92	0.42	22.89
Radial	–1.24	–0.24	0.5	9.11
Ulnar	1.21	0.26	–0.42	11.2

Abbreviation: PLA, polylactic acid.

Besides, the von Mises stress has decreased from 31. 58 to 19.98 MPa (peak stress value in flexion), making it safer if the applied load is 8% of the Vanwearingen load (highest isometric strength of a healthy person). This improvement, meanwhile, has come at the expense of higher manufacturing costs, comprising increased material utilization and longer building time. A greater thickness also means a heavier splint, which can make it more difficult for the patient to do daily duties and cause discomfort.

The projected study makes an effort to simulate how a patient's hand might behave with a splint in real life. There are some specific dynamics, though, that are oversimplified and ignored in this work. For instance, there is no evidence in the literature addressing wrist joints with stroke, making it difficult to determine what the intensity of the loads should be. Because of this knowledge gap, the authors assumed that the decrease in strength in a stroke-affected wrist is equivalent to that of an arthritic-affected wrist. So, it would be intriguing in future work to include the actual forces that a patient with stroke could deliberately generate to the splint in realistic deployment. Furthermore, one of the drawbacks of this study is that the manufacturer data and literature studies are utilized to get the mechanical properties utilized in FE simulations. This information is gathered under ideal settings; thus, they might not accurately represent actual situations. Hence, the mechanical properties have been used without taking the splint's anisotropic behavior (because of the 3D printing) into account. Future research should examine the implications of anisotropy. Moreover, the splint in this study is devised that can sustain a light load and accommodate tolerable deformations. The stresses in the splint, however, could occasionally exceed the maximum strength of the material when the loads are increased. Hence, it is crucial to reinforce it by investigating more materials with a higher modulus of elasticity, increasing the splint thickness, introducing novel lattice structures into the splint, etc. It is also significant to keep in mind that the loads and boundary conditions used significantly govern the outcomes of an FE simulation. There is no evidence in the literature on wrist joints with stroke, so it is impossible to determine what the degree of the loads should be. The authors assumed that the muscle impairment in a wrist afflicted by a stroke is quite similar

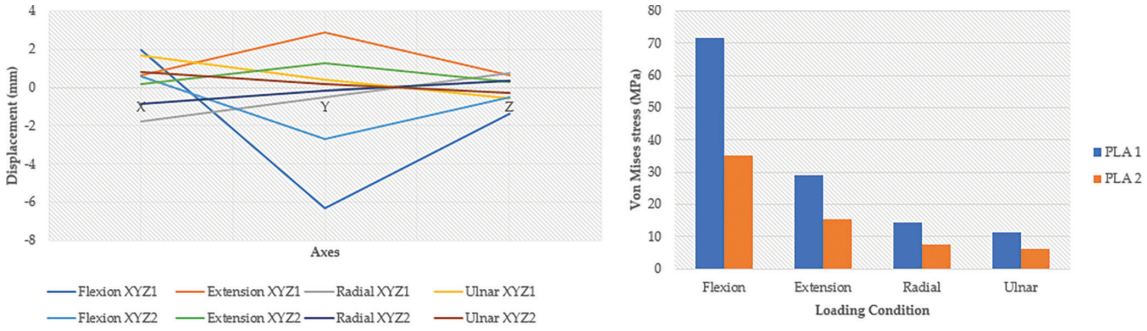

Figure 10: PLA-based 1- and 2-mm-thick hand splint configurations. (a) Displacement X, Y, and Z and (b) von Mises stress. Abbreviation: PLA, polylactic acid.

Table 8: Results for the 2- and 3- mm-thick PLA splint at their maximum loads.

PLA	X (mm)	Y (mm)	Z (mm)	von Mises stress (MPa)
Applied load (thickness)				
12% (2 mm)				
Flexion	0.91	−4.05	−0.74	52.58
Extension	0.27	1.92	0.42	22.89
Radial	−1.24	−0.24	0.5	9.11
Ulnar	1.21	0.26	−0.42	11.2
20% (3 mm)				
Flexion	0.69	−4.1	0.07	54.43
Extension	0.2	1.99	0.44	23.52
Radial	−1.33	−0.17	0.53	11.75
Ulnar	1.31	0.24	−0.46	10.19

Abbreviation: PLA, polylactic acid.

to that of a wrist influenced by arthritis as a consequence of the absence of information. It is also extremely important to keep in mind that the outcomes of FE simulations are entirely reliant on the assumed loads and constraints.

CONCLUSION

In this study, hand orthoses composed of various 3D printing materials and demonstrating varying thicknesses are examined using FE analysis. Numerical simulations serve as tools to compare the resulting stresses and displacements. The splint model is constituted by digitizing a real wrist with a noncontact scanner that uses 3D scanning technology. This study has documented that the PLA-based 2-mm-thick hand orthosis has shown better performance if the applied load is within 11.8, 6.7, 9.1, and 7.9 N in flexion, extension, radial, and ulnar loading scenarios, respectively. The PLA has been chosen because it has shown more robust and stable performance in terms of average displacement as compared to other materials. However, the von Mises stresses in all the materials are below their yield strength limits if the applied loads to the splints are 8% of those applied by healthy people. The results have also shown that the PLA splint has 38.6%, 38.8%, 38.5%, and 38.7% less displacement than ABS in flexion, extension, radial, and ulnar movements respectively. A physical prototype of the 2-mm-thick hand splint made of PLA material is also produced. The findings of this study confirm the prospects investigated by previous investigators and assist in assuaging design engineers' main concerns about 3D printing. Indeed, if the right material is chosen for the wrist splint's design, it can endure the stresses that a patient would put on it in an actual situation. The research also shows that there is a lot of room for an investigation into 3D-printed splints. It would also be beneficial to examine more designs, albeit doing so would necessitate participants and incur expenses in terms of material cost, design time, and therapeutic time. Human studies will eventually be required

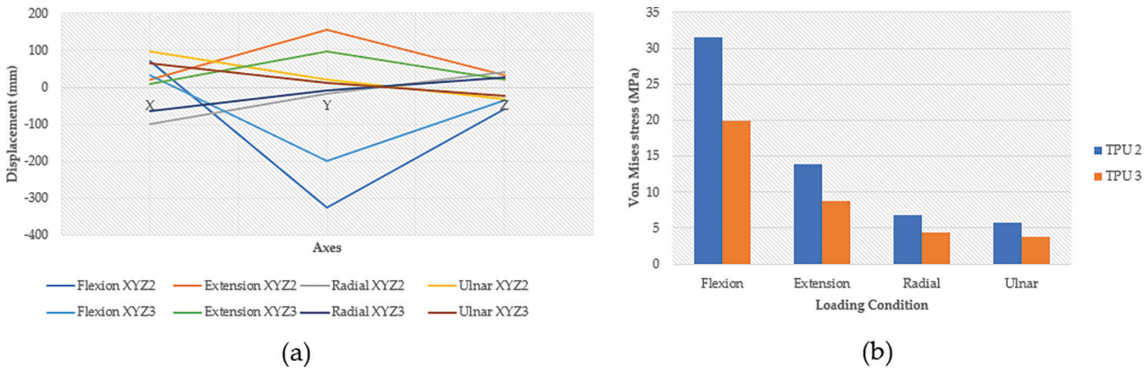

Figure 11: TPU-based 2- and 3-mm-thick hand splint designs. (a) Displacement X, Y, and Z and (b) von Mises stress. Abbreviation: TPU, thermoplastic polyurethanes.

to prove the usefulness and affordability of 3D-printed splints. It is also necessary to look into the material's long-term capabilities to determine the appropriate service life. In the future task, additional testing of the 3D-printed prototype of the splint will be done under realistic circumstances to verify the results of the FE analysis. These tests are outside the scope of this study due to time and financial limitations; however, the setup is being built for future experiments. The authors are also developing a dynamic exoskeleton for hand rehabilitation that can be used both in a hospital environment and at home for patient training.

This analysis has thus led us to the conclusion that a hand splint made of PLA with a 2-mm thickness can minimize material costs without diminishing the splint's performance. Furthermore, it is recommended that the 3D-printed hand splint would work effectively if an appropriate material and splint thickness are chosen.

FUNDING

This research was funded by the King Salman Center for Disability Research through Research Group no KSRG-2022-060.

AUTHOR CONTRIBUTIONS

U.U. and S.H.M. conceptualized the study. U.U., S.H.M., and K.M. performed the methodology; U.U. and S.H.M. were in charge of the software; K.M. and H.A. validated the study; U.U. and H.A. performed formal analysis; H.A. took care of the investigation; U.U., S.H.M., and H.A. were responsible for the resources; H.A. performed data curation; S.H.M. and K.M. prepared original draft; U.U., S.H.M., and H.A. reviewed and edited the manuscript; K.M. and H.A. performed visualization; H.A. supervised the project; U.U. and S.H.M. took care of project administration; U.U., S.H.M., and H.A. performed funding acquisition. All authors have read and agreed to the published version of the manuscript.

CONFLICTS OF INTEREST

The authors declare no conflicts of interest in association with the present study.

ACKNOWLEDGMENTS

The authors extend their appreciation to the King Salman Center for Disability Research for funding this work through Research Group no KSRG-2022-060.

DATA AVAILABILITY STATEMENT

The data presented in this study are available in the article.

REFERENCES

Abdelbasset W.K. and Sulieman A. (2022). An overview on low back pain and functional disability: associated risk factors and management. *J. Disabil. Res.,* 1, 19-22. https://doi.org/10.57197/JDR-2022-0004.

Acrylonitrile Butadiene Styrene (ABS Plastic): Uses, Properties & Structure. Available online: https://omnexus.specialchem.com/selection-guide/acrylonitrile-butadiene-styrene-abs-plastic (accessed on 12 March 2023).

Aimar A., Palermo A. and Innocenti B. (2019). The role of 3D printing in medical applications: a state of the art. *J. Healthc. Eng.*, 2019, e5340616. https://doi.org/10.1155/2019/5340616.

Alqahtani B.A., Alenazi A.M., Hoover J.C., Alshehri M.M., Alghamdi M.S., Osailan A.M., et al. (2020). Incidence of stroke among Saudi population: a systematic review and meta-analysis. *Neurol. Sci.,* 41, 3099-3104. https://doi.org/10.1007/s10072-020-04520-4.

Andringa A., van de Port I. and Meijer J.-W. (2013). Long-term use of a static hand-wrist orthosis in chronic stroke patients: a pilot study. *Stroke Res. Treat.,* 2013, 546093. https://doi.org/10.1155/2013/546093.

Bakraa R., Aldhaheri R., Barashid M., Benafeef S., Alzahrani M., Bajaba R., et al. (2021). Stroke risk factor awareness among populations in Saudi Arabia. *Int. J. Gen. Med.*, 14, 4177-4182. https://doi.org/10.2147/IJGM.S325568.

Barrios-Muriel J., Romero-Sánchez F., Alonso-Sánchez F.J. and Salgado D.R. (2020). Advances in orthotic and prosthetic manufacturing: a technology review. *Materials (Basel),* 13, 295. https://doi.org/10.3390/ma13020295.

Bhave A., Sodhi N., Anis H.K., Ehiorobo J.O. and Mont M.A. (2019). Static progressive stretch orthosis-consensus modality to treat knee stiffness – rationale and literature review. *Ann. Transl. Med.*, 7, S256. https://doi.org/10.21037/atm.2019.06.55.

Blaya F., Pedro P.S., Silva J.L., D'Amato R., Heras E.S. and Juanes J.A. (2018). Design of an orthopedic product by using additive manufacturing technology: the arm splint. *J. Med. Syst.*, 42, 54. https://doi.org/10.1007/s10916-018-0909-6.

Broeks J.G., Lankhorst G.J., Rumping K. and Prevo A.J. (1999). The long-term outcome of arm function after stroke: results of a follow-up study. *Disabil. Rehabil.*, 21, 357-364. https://doi.org/10.1080/096382899297459.

Cazon A., Kelly S., Paterson A.M., Bibb R.J. and Campbell R.I. (2017). Analysis and comparison of wrist splint designs using the finite element method: multi-material three-dimensional printing compared to typical existing practice with thermoplastics. *Proc. Inst. Mech. Eng. H.,* 231, 881-897. https://doi.org/10.1177/0954411917718221.

Chen Y., Yu J., Ling Y., Yao S., Jiang X., Hu D., et al. (2022). Comprehensive analysis of mechanical properties of microcellular polypropylene: experiment and simulation. *Polym. Test.*, 116, 107812. https://doi.org/10.1016/j.polymertesting.2022.107812.

Choi H.-W., Kang I., Noh G., Seo A. and Lee J.-M. (2019). Finite element analysis of wrist orthosis with 3D printing. *J. Korean Soc. Radiol.,* 13, 947-953. https://doi.org/10.7742/JKSR.2019.13.7.947.

Garrett J.W. (1971). The adult human hand: some anthropometric and biomechanical considerations. *Hum. Factors,* 13, 117-131. https://doi.org/10.1177/001872087101300204.

Glinsky J., Harvey L., Korten M., Drury C., Chee S. and Gandevia S.C. (2008). Short-term progressive resistance exercise may not be effective at increasing wrist strength in people with tetraplegia: a randomised controlled trial. *Aust. J. Physiother.*, 54, 103-108. https://doi.org/10.1016/S0004-9514(08)70043-6.

Handayani S.U., Fahrudin M., Mangestiyono W. and Alaya Fadlu H. (2021). Mechanical properties of commercial recycled polypropylene from plastic waste. *J. Vocat. Stud. Appl. Res.*, 3, 1-4.

Huysamen H.W., Kinnear W.A., Fonternel T.E., Turton E., Yadroitsava I. and Yadroitsev I. (2020). 3D printed laryngoscope for endotracheal intubation. *South African J. Ind. Eng.*, 31, 209-217. https://doi.org/10.7166/31-3-2446.

INTAMSYS. Intamsys FUNMAT HT 3D Printer. Available online: https://www.intamsys.com/funmat-ht-3d-printer/ (accessed on 27 June 2021).

INTAMSYS. High-Performance Materials. Available online: https://www.intamsys.com/high-performance-materials/ (accessed on 13 January 2022).

INTAMSYS. Intamsys Funmat HT Enhanced – Vision Miner. Available online: https://visionminer.com/products/funmat-ht-enhanced (accessed on 15 March 2023).

Keane, P. (2021). PETG vs PLA: How Do They Compare (accessed on 9/3/2023). https://www.wevolver.com/article/petg-vs-pla-how-do-they-compare.

Krumm D., Schwanitz S. and Odenwald S. (2022). spinfortec2022: Tagungsband zum 14. *Symposium der Sektion Sportinformatik und Sporttechnologie der Deutschen Vereinigung für Sportwissenschaft (dvs), Chemnitz 29. -30. September 2022*.

Kubasad P.R., Gawande V.A., Todeti S.R., Kamat Y.D. and Vamsh, N. (2020). Design and analysis of a passive ankle foot orthosis by using transient structural method. *J. Phys. Conf. Ser.*, 1706, 012203. https://doi.org/10.1088/1742-6596/1706/1/012203.

Lalegani Dezaki M., Mohd Ariffin M.K.A. and Hatami S. (2021). An overview of fused deposition modelling (FDM): research, development and process optimisation. *Rapid Prototyp. J.*, 27, 562-582. https://doi.org/10.1108/RPJ-08-2019-0230.

León-Calero M., Reyburn Valés S.C., Marcos-Fernández Á. and Rodríguez-Hernandez J. (2021). 3D printing of thermoplastic elastomers: role of the chemical composition and printing parameters in the production of parts with controlled energy absorption and damping capacity. *Polymers*, 13, 3551. https://doi.org/10.3390/polym13203551.

Li J. and Tanaka H. (2018). Rapid customization system for 3D-printed splint using programmable modeling technique – a practical approach. *3D Print. Med.,* 4, 5. https://doi.org/10.1186/s41205-018-0027-60.

Lu P., Liao Z., Zeng Q., Chen H., Huang W., Liu Z., et al. (2021). Customized three-dimensional-printed orthopedic close contact casts for the treatment of stable ankle fractures: finite element analysis and a pilot study. *ACS Omega*, 6, 3418-3426. https://doi.org/10.1021/acsomega.0c06031.

Łukaszewski K., Wichniarek R. and Górski F. (2020). Determination of the elasticity modulus of additively manufactured wrist hand orthoses. *Materials*, 13, 4379. https://doi.org/10.3390/ma13194379.

Luximon Y., Shah P. and Hashmi H. (2019). Aesthetic considerations in the ortho-prosthetic design process. In: *Conference Proceedings of the Academy for Design Innovation Management*, vol. 2. Academy for Design Innovation Management, London.

MedScan3D. Market News: How Medical 3D Printing Revolutionalise Healthcare Industry. February 23, 2023. (accessed on 14/3/2023). https://www.medscan3d.ie/market-news-how-medical-3d-printing-revolutionalise-healthcare-industry/.

Mian S.H. and Al-Ahmari A. (2019). Comparative analysis of different digitization systems and selection of best alternative. *J. Intell. Manuf.,* 30, 2039-2067. https://doi.org/10.1007/s10845-017-1371-x.

Mian S.H., Moiduddin K., Elseufy S.M. and Alkhalefah H. (2022). Adaptive mechanism for designing a personalized cranial implant and its 3D printing using PEEK. *Polymers (Basel)*, 14, 1266. https://doi.org/10.3390/polym14061266.

Miller E.L., Murray L., Richards L., Zorowitz R.D., Bakas T., Clark P., et al. (2010). Comprehensive overview of nursing and interdisciplinary rehabilitation care of the stroke patient: a scientific statement from the American Heart Association. *Stroke*, 41, 2402-2448. https://doi.org/10.1161/STR.0b013e3181e7512b.

Oksiuta Z., Jalbrzykowski M., Mystkowska J., Romanczuk E. and Osiecki T. (2020). Mechanical and thermal properties of polylactide (PLA) composites modified with Mg, Fe, and polyethylene (PE) additives. *Polymers (Basel)*, 12, 2939. https://doi.org/10.3390/polym12122939.

Paton J., Jones, R.B., Stenhouse E. and Bruce G. (2007). The physical characteristics of materials used in the manufacture of orthoses for patients with diabetes. *Foot Ankle Int.*, 28, 1057-1063. https://doi.org/10.3113/FAI.2007.1057.

PETG (Polyethylene Terephthalate Copolyester). Technical Data Sheet by SD3D; SD3D (accessed on 9/3/2023). https://www.sd3d.com/wp-content/uploads/2017/06/MaterialTDS-PETG_01.pdf.

PETG 3D Printing Material - Proto 3000 (accessed on 12/3/2023). https://proto3000.com/materials/petg-3d-printing-filament-material/.

Petousis M., Vidakis N., Mountakis N., Karapidakis E. and Moutsopoulou A. (2023). Functionality versus sustainability for PLA in MEX 3D printing: the impact of generic process control factors on flexural response and energy efficiency. *Polymers (Basel),* 15, 1232. https://doi.org/10.3390/polym15051232.

Robert A.A. and Zamzami M.M. (2014). Stroke in Saudi Arabia: a review of the recent literature. *Pan Afr. Med. J.,* 17, 14. https://doi.org/10.11604/pamj.2014.17.14.3015.

Schultz-Johnson K. (2002). Static progressive splinting. *J. Hand Ther.*, *15*, 163-178. https://doi.org/10.1053/hanthe.2002.v15.015016.

Sepahi M.T., Abusalma H., Jovanovic V. and Eisazadeh H. (2021). Mechanical properties of 3D-printed parts made of polyethylene terephthalate glycol. *J. Mater. Eng. Perform.*, 30, 6851-6861. https://doi.org/10.1007/s11665-021-06032-4.

Siddiqui M.I.H., Arifudin L., Alnaser I.A. and Alluhydan K. (2023). Numerical investigation on the performance of prosthetic running blades by using different materials. *J. Disabil. Res.,* 2, 6-13. https://doi.org/10.57197/JDR-2023-0001.

Travieso-Rodriguez J.A., Jerez-Mesa R., Llumà J., Traver-Ramos O., Gomez-Gras G. and Roa Rovira J.J. (2019). Mechanical properties of 3D-printing polylactic acid parts subjected to bending stress and fatigue testing. *Materials (Basel),* 12, 3859. https://doi.org/10.3390/ma12233859.

Vaish A. and Vaish R. (2018). 3D printing and its applications in orthopedics. *J. Clin. Orthop. Trauma*, 9, S74-S75. https://doi.org/10.1016/j.jcot.2018.02.003.

Vanswearingen J. (1983). Measuring wrist muscle strength. *J. Orthop. Sports Phys. Ther.,* 4, 217-228. https://doi.org/10.2519/jospt.1983.4.4.217.

Volz R.G., Lieb M. and Benjamin J. (1980). Biomechanics of the wrist. *Clin. Orthop. Relat. Res.,* 149, 112-117.

Vukasovic T., Vivanco J.F., Celentano D. and García-Herrera C. (2019). Characterization of the mechanical response of thermoplastic parts fabricated with 3D printing. *Int. J. Adv. Manuf. Technol.,* 104, 4207-4218. https://doi.org/10.1007/s00170-019-04194-z.

Walbran M., Turner K. and McDaid A.J. (2016). Customized 3D printed ankle-foot orthosis with adaptable carbon fibre composite spring joint. *Cogent Eng.,* 3, 1227022. https://doi.org/10.1080/23311916.2016.1227022.

Wyleżoł M. (2018). Hybrid modeling methods of cranial implants. *Adv. Sci. Technol. Res. J.,* 12, 35-47. https://doi.org/10.12913/22998624/99039.

Yavuz G.A., Kiral B.G., Katre S. and Atilla D. (2021). Effects of topology and material on mechanical properties of structures produced by the additive manufacturing method. *DEUFMD*, 23, 755-765. https://doi.org/10.21205/deufmd.2021236905.

Youm Y., McMurthy R.Y., Flatt A.E. and Gillespie T.E. (1978). Kinematics of the Wrist. I. An experimental study of radial–ulnar deviation and flexion-extension. *J. Bone Joint Surg. Am.,* 60, 423-431.